



































BURSTT: Bustling Universe Radio Survey Telescope in Taiwan

HSIU-HSIEN LIN ^{1,2} KAI-YANG LIN ¹ CHAO-TE LI ¹ YAO-HUAN TSENG ¹ HOMIN JIANG ¹ JEN-HUNG WANG ¹
JEN-CHIEH CHENG,¹ UE-LI PEN ^{1,2,3,4,5} MING-TANG CHEN ^{6,1} PISIN CHEN ^{7,8} YAOCHENG CHEN ^{7,8}
TOMOTSUGU GOTO ⁹ TETSUYA HASHIMOTO ¹⁰ YUH-JING HWANG ¹ SUN-KUN KING,¹ DEREK KUBO,⁶
CHUNG-YUN KUO ^{8,7} ADAM MILLS,⁶ JIWOON NAM ^{7,8} PETER OSHIRO,⁶ CHANG-SHAO SHEN ¹ HSIEN-CHUN TSENG,¹
SHIH-HAO WANG ^{7,8} VIGO FENG-SHUN WU,¹ GEOFFREY BOWER ⁶ SHU-HAO CHANG,¹ PAI-AN CHEN,¹
YING-CHIH CHEN,^{7,8} YI-KUAN CHIANG ¹ ANATOLI FEDYNITCH ¹¹ NINA GUSINSKAIA ^{4,2} SIMON C.-C. HO ⁹
TIGER Y.-Y. HSIAO ^{9,12} CHIN-PING HU ¹³ YAU DE HUANG ¹ JOSÉ MIGUEL JÁUREGUI GARCÍA ²
SEONG JIN KIM ⁹ CHENG-YU KUO ¹⁴ DECMEEND FANG-JIE LING,¹⁵ ALVINA Y. L. ON ^{9,10,16}
JEFFREY B. PETERSON ¹⁷ BJORN JASPER R. RAQUEL ^{10,18} SHIH-CHIEH SU,^{7,8} YURI UNO ¹⁰ COSSAS K.-W. WU,⁹
SHOTARO YAMASAKI ¹⁰ AND HONG-MING ZHU ²

- ¹*Institute of Astronomy and Astrophysics, Academia Sinica, 11F of AS/NTU Astronomy-Mathematics Building, No.1, Sec. 4, Roosevelt Rd, Taipei 10617, Taiwan, R.O.C.*
- ²*Canadian Institute for Theoretical Astrophysics, 60 St. George Street, Toronto, ON M5S 3H8, Canada*
- ³*Canadian Institute for Advanced Research, 180 Dundas St West, Toronto, ON M5G 1Z8, Canada*
- ⁴*David D Dunlap Institute for Astronomy and Astrophysics, University of Toronto, 50 St George Street, Toronto, ON M5S 3H4, Canada*
- ⁵*Perimeter Institute of Theoretical Physics, 31 Caroline Street North, Waterloo, ON N2L 2Y5, Canada*
- ⁶*Institute of Astronomy and Astrophysics, Academia Sinica, 645 N Aohoku Pl, Hilo, HI 96720 USA*
- ⁷*Department of Physics, National Taiwan University, No. 1, Sec. 4, Roosevelt Rd., Taipei 10617, Taiwan, R.O.C.*
- ⁸*Leung Center for Cosmology and Particle Astrophysics, National Taiwan University, No. 1, Sec. 4, Roosevelt Rd., Taipei 10617, Taiwan, R.O.C.*
- ⁹*Institute of Astronomy, National Tsing Hua University, 101 Section 2 Kuang-Fu Road, Hsinchu 30013, Taiwan (ROC)*
- ¹⁰*Department of Physics, National Chung Hsing University, No. 145, Xingda Rd., South Dist., Taichung 40227, Taiwan (R.O.C.)*
- ¹¹*Institute of Physics, Academia Sinica, Taipei, 11529, Taiwan*
- ¹²*Department of Physics and Astronomy, Johns Hopkins University, Baltimore, MD 21218, USA*
- ¹³*Department of Physics, National Changhua University of Education, Changhua, 50007, Taiwan*
- ¹⁴*Physics Department, National Sun Yat-Sen University, No. 70, Lien-Hai Road, Kaosiung City 80424, Taiwan, R.O.C.*
- ¹⁵*Department of Physics, National Tsing Hua University, 101 Section 2 Kuang-Fu Road, Hsinchu 30013, Taiwan (ROC)*
- ¹⁶*Mullard Space Science Laboratory, University College London, Holmbury St Mary, Surrey RH5 6NT, UK*
- ¹⁷*Department of Physics, Carnegie Mellon University, 5000 Forbes Ave. Pittsburgh PA 15213 USA*
- ¹⁸*Department of Earth and Space Sciences, Rizal Technological University, Boni Avenue, Mandaluyong, 1550 Metro Manila, Philippines*

(Received TBD; Revised TBD; Accepted TBD)

ABSTRACT

Fast Radio Bursts (FRBs) are bright millisecond-duration radio transients that appear about 1,000 times per day, all-sky, for a fluence threshold 5 Jy ms at 600 MHz. The FRB radio-emission physics and the compact objects involved in these events are subjects of intense active debate. To better constrain source models, the Bustling Universe Radio Survey Telescope in Taiwan (BURSTT) is optimized to discover and localize a large sample of rare, high-fluence, nearby FRBs. This is the population most amenable to multi-messenger, multi-wavelength follow-up, allowing deeper understanding of source mechanisms. BURSTT will provide horizon-to-horizon sky coverage with a half power field-of-view (FoV) of $\sim 10^4$ deg², a 400 MHz effective bandwidth between 300-800 MHz, and sub-arcsecond localization, made possible using outrigger stations hundreds to thousands of km from the main array. Initially, BURSTT will employ 256 antennas. After tests of various antenna designs and optimization of system performance we plan to expand to 2048 antennas. We estimate that BURSTT-256 will detect

and localize ~ 100 bright (≥ 100 Jy ms) FRBs per year. Another advantage of BURSTT’s large FoV and continuous operation will be greatly enhanced monitoring of FRBs for repetition. The current lack of sensitive all-sky observations likely means that many repeating FRBs are currently cataloged as single-event FRBs.

Keywords: radio transient sources, astronomical instrumentation, wide-field telescopes, very long baseline interferometry

1. INTRODUCTION

Fast Radio Bursts (FRBs) are bright (~ 1 Jy), millisecond flashes of radio light of uncertain astrophysical origin (Lorimer et al. 2007; Tendulkar et al. 2017; Macquart et al. 2020). With the fluence threshold above 5 Jy ms at 600 MHz, the all-sky occurrence rates of FRBs is $\sim 1,000$ per day (e.g., CHIME/FRB Collaboration et al. (2018, 2021)). The spatial distribution is independent of the galactic latitude (Josephy et al. 2021; Bhandari et al. 2018).

The nature of FRBs, including their emission mechanism, central object type, and environment, is one of the most perplexing enigmas in astrophysics. Deepening the mystery, about 4 percent of FRB sources emit multiple bursts (CHIME/FRB Collaboration et al. 2021), the so-called “repeaters” (e.g., Spitler et al. (2016)), while for most FRBs only one burst is observed (e.g., Petroff et al. (2019); CHIME/FRB Collaboration et al. (2021)). A few FRBs have been reported with periodicities ranging from sub-seconds to several months (CHIME/FRB Collaboration et al. 2022; Chime/Frb Collaboration et al. 2020; Rajwade et al. 2020). It is so far unclear whether repeaters and non-repeaters originate from astrophysically different populations and whether there are multiple channels for FRB formation (Platts et al. 2019; Hashimoto et al. 2020).

About two dozen FRBs have been associated with a particular host galaxy (Chatterjee et al. 2017; Bhandari et al. 2020; Heintz et al. 2020; Bhandari et al. 2022), and a few repeaters have been pinpointed inside the host galaxy through Very-Long Baseline Interferometry (VLBI) (Marcote et al. 2017, 2020; Kirsten et al. 2022). Two repeating FRBs are associated with persistent radio sources (Marcote et al. 2017; Niu et al. 2022), which show complicated polarization properties (Michilli et al. 2018; Anna-Thomas et al. 2022; Dai et al. 2022).

Because only a small number of FRB’s have been associated with host galaxies the distance to these sources has so far not been available so luminosity function of FRBs is currently poorly constrained (Luo et al. 2018).

Although almost fifteen years have passed since their discovery (Lorimer et al. 2007), there is no consensus about their origin despite an increasing number of recent detections (Platts et al. 2019; CHIME/FRB Collaboration et al. 2021). Beyond the central questions of the source composition and emission mechanism, it has been suggested that FRBs could be used to address key issues in cosmology and physics, including dark energy (e.g., Liu et al. (2019); Hashimoto et al. (2019)), dark matter (e.g., Muñoz et al. (2016); Leung et al. (2022)), testing of the general relativity (e.g., Wei et al. (2015); Hashimoto et al. (2021)), and the missing baryon problem (e.g., Muñoz & Loeb (2018); Macquart et al. (2020)).

There have been three major challenges in revealing the physical origins of FRBs: (i) low detection probability. Existing telescopes have limited field of view (FoV), but FRBs randomly appear on the sky, so the great majority of detectable FRBs are currently missed., (ii) poor localization to their host, due to the insufficient spatial resolution of existing radio telescopes, and (iii) The high antenna gain of current telescopes means that FRBs currently detected are often too distant to conduct multi-wavelength/multi-messenger observations to identify their progenitors, host galaxies, and simultaneous emission counterparts. All of these issues arise because existing radio telescopes are not tailored for FRBs.

The proposed Bustling Universe Radio Survey Telescope in Taiwan (BURSTT) will address all these problems by detecting high-fluence (bright) FRBs in the nearby Universe. Because of the relatively small cosmic volume in the nearby universe these are rare, so we have maximized the FoV to increase the detection rate. BURSTT is a unique fisheye radio software telescope, with which we will observe at least 25 times more sky than any existing radio observatory, except the Survey for Transient Astronomical Radio Emission 2 (STARE2) (Bochenek et al. 2020a), which has a much lower sensitivity than BURSTT. By viewing so much more sky than other telescopes, and hence detecting a larger sample of bright and nearby sources, BURSTT will be unique in identifying multi-frequency (i.e. optical and X-ray/gamma-ray) and multi-messenger (gravitational-wave and neutrino) counterparts. In addition, BURSTT-2048 will add substantially to the the overall world-wide FRB detection rate.

In this paper, the scientific objectives of BURSTT are shown in Section 2. The potential technical aspects are illustrated in Section 3. The work is summarized in Section 4.

2. SCIENCE OBJECTIVES

2.1. *The extremely wide field of view of BURSTT*

To achieve a complete census of FRBs, monitoring observations of the nearby Universe with a very wide FoV are required (Bochenek et al. 2020a; Connor et al. 2021).

For any array of antennas, the FoV is inversely proportional to the effective collecting area of the array, so the wide field of BURSTT means it will have a smaller collecting area than many previous telescopes. In estimating the detection rate (see below) the area and FOV factors partially compensate and the resulting detection rate is not strongly dependent on the choice of FoV. However, for the wide field (low collecting area) telescope, the detected sources are on average closer.

The redshift of CHIME/FRB sample is in the range of 0.3-0.5 (Rafei-Ravandi et al. 2021). The CHIME/FRB team is adding outriggers to CHIME, which will localize many FRB events in this redshift range (Cassanelli et al. 2022; Mena-Parra et al. 2022). For many of these, optical follow-up observations will be needed to get the redshift of the host galaxy. In contrast, we anticipate the median redshift of the BURSTT FRB sample will be in the range of 0.03-0.05. This means that many of the BURSTT host galaxies will be present in existing optical redshift survey catalogs (Karachentsev et al. 2013; Cutri et al. 2003; Bilicki et al. 2014, 2016; Dey et al. 2019) allowing immediate redshift determination without the need for follow-up observations. This will allow for a rapid improvement in the measured FRB luminosity function (Shin et al. 2022).

To estimate the system equivalent flux density (SEFD) sensitivity of the BURSTT, we assume a conservative system temperature (T_{sys}) of ~ 150 K, achievable with commercially-available LNAs, and an effective area for 256 antennas of ~ 100 m² at 600 MHz. The corresponding SEFD is ~ 5000 Jy. For an FRB with a duration of 1 ms across 400 MHz bandwidth with a fluence of 100 Jy ms, the corresponding signal-to-noise ratio (S/N) is ~ 12 . In the future, we hope to achieve T_{sys} of 50 K, which will improve the sensitivity.

To estimate the event rate, we assume a Euclidian distribution to scale from a previously measured reference rate,

$$N(S) = N_0 \left(\frac{S}{S_0} \right)^{-1.5}, \quad (1)$$

where $N(S)$ is the event rate above fluence S , N_0 is the reference rate above reference fluence S_0 . We use the reference event rate reported by CHIME (CHIME/FRB Collaboration et al. 2021), 300 FRBs per day per sky, with $S_0 = 5$ Jy ms at 600 MHz, and two additional constraints: scattering time at 600 MHz below 10 ms and DM above 100 pc cm⁻³. The FoV of BURSTT is $\sim 10^4$ deg² or 0.24 sky. Thus, we estimate that BURSTT-256 can detect ~ 100 bright FRBs per year with the threshold of fluence higher than 100 Jy ms at 600 MHz. Note that the CHIME FRB rate is at the low end of published rate estimates, making our estimate a conservative one.

The properties of repeating FRBs are poorly constrained (e.g., Fonseca et al. (2020)) because only a small number have been detected. Uncertain parameters include the event rate and its dependence on flux density, the possibility of non-Poisson distribution of events (Oppermann et al. 2018), and the host environment of these FRBs. With its all-sky coverage BURSTT will likely uncover a larger fraction of repeaters, sharply localize the sources and provide the detailed data for each received pulse. This should substantially improve our understanding of repeating FRBs.

Figure 1 shows the FoV versus the SEFD and the effective area for the existing, planned, and future-concept FRB surveys, including CHIME (CHIME/FRB Collaboration et al. 2018), Australian Square Kilometre Array Pathfinder (ASKAP) (Macquart et al. 2010), the Canadian Hydrogen Observatory and Radio-transient Detector (CHORD) (Vanderlinde et al. 2019), STARE2 (Bochenek et al. 2020a), Galactic Radio Explorer (GREx) (Connor et al. 2021), Deep Synoptic Array 2000 (DSA-2000)¹, Five-hundred-meter Aperture Spherical Telescope (FAST) (Jiang et al. 2019), Green Bank Telescope (GBT) (Connor et al. 2016), the Hydrogen Intensity and Real-time Analysis eXperiment (HIRAX) (Newburgh et al. 2016), MeerKAT (Rajwade et al. 2021), Parkes (Petroff et al. 2014), Packed Ultra-wideband Mapping Array (PUMA) (Slosar et al. 2019), Square Kilometre Array Phase 1 (SKA-1) (Braun et al. 2019), SKA-2 (Torchinsky et al. 2016), and Very Large Array (VLA) (Law et al. 2018).

¹ <https://www.deepsynoptic.org/overview>

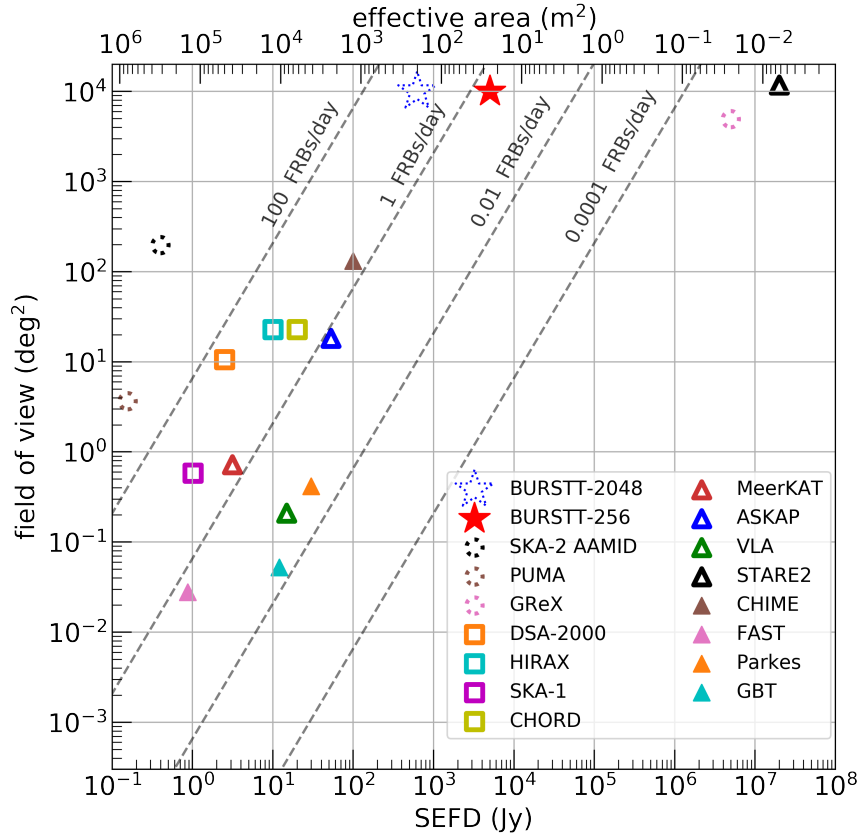


Figure 1. Comparison of BURSTT’s FoV, effective collecting area, sensitivity (SEFD), and FRB detection rate (dashed lines) vs. existing (solid), planned (outline), and future-concept (dotted circle) observatories. Rates(dashed lines) were calibrated to CHIME, assuming Euclidean rates and 400 MHz bandwidth. Open triangles are sparse interferometers, which provide arcsecond localization and would require correlator upgrades to achieve these rates. The rate is a hypothetically upper limit, with the assumption of 24/7 FRB searches (which only CHIME/FRB does) as well as the optimal FRB searches with coherently beam-forming for the interferometry (ASKAP, VLA). BURSTT is unique in the large FoV with enough sensitivity to detect a large sample of bright and nearby FRBs.

2.2. Immediate localization by BURSTT

The critical step to reveal the origin of FRBs is to measure the accurate positions of FRBs, i.e., localization, to identify their progenitors. Out of more than 600 FRBs published to date (Petroff et al. 2016; CHIME/FRB Collaboration et al. 2021), there has been only one successful case of localization to a stellar progenitor, which identified the FRB as a Galactic magnetar, SGR 1935+2154 (CHIME/FRB Collaboration et al. 2020; Bochenek et al. 2020b; Kirsten et al. 2021), and clearly indicates the magnetar as the progenitor of this particular FRB.

Recently, three repeating FRB sources were localized in nearby star-forming regions of galaxies (Bassa et al. 2017; Marcote et al. 2020; Piro et al. 2021). This may indicate young stellar populations as a possible origin of repeating FRBs. In contrast, another repeating FRB source was localized in the globular cluster in M81, a nearby galaxy, suggesting FRB origins are to be found in old stellar populations (Kirsten et al. 2022). This apparent contradiction could be due to the small sample size. A statistical relation between localized FRBs and their host galaxies has been studied (Li & Zhang 2020), while more localized samples are necessary to understand the host environments. BURSTT will detect and localize ~ 100 bright FRB per year to further distinguish their local environment, and such statistics are important to understand the population (Leung et al. 2021; Mena-Parra et al. 2022; Cassanelli et al. 2022).

Very-Long Baseline Interferometry (VLBI) along with outrigger stations has been proposed to localize both non-repeating and repeating FRBs (Cassanelli et al. 2022). For the latter, the European VLBI Network (EVN) has localized several repeating FRBs to their hosts (Marcote et al. 2020; Kirsten et al. 2022). Along with the VLBI outrigger stations, BURSTT can localize FRBs to their hosts. For instance, an outrigger located a few hundred km

away from the main array will provide ~ 1 arcsecond localization for the host galaxy. Such localization will lead to the identification of FRB hosts and potentially the progenitors of the nearby sources, allowing us to understand the nature of FRBs.

2.3. Long-term high cadence monitoring with BURSTT

The observational classification of FRBs as repeating and non-repeating has caused a major problem over the past decade: non-repeating FRBs can be contaminated by repeating FRBs since this classification is a purely observational definition (Ai et al. 2021; Chen et al. 2022). Due to limited observational time, a significant fraction of repeating bursts may be missed and thus such FRBs could be misclassified as non-repeating FRBs. However, long-term monitoring observations are extremely expensive and difficult using current and planned radio telescopes.

BURSTT, on the other hand, will monitor a fixed large patch of the sky all the time (See Table 1). This is essential for non-stop monitoring of repeating and non-repeating FRBs. Repeating FRBs could originate from the repeating activities of progenitors, such as pulsars and magnetars, while non-repeating FRBs may be generated by catastrophic one-off events, such as compact merger systems (Platts et al. 2019). BURSTT will thus provide a great statistics of source repetitions as well as precise constraints on apparent non-repetition of one-off events.

BURSTT can monitor the northern hemisphere at least 7 hours per day (24 hours for North pole and ~ 7 hours for the equator). BURSTT's longer monitoring minimizes the chance it will miss any repeating FRBs, which will resolve the missing repeating FRB problem. Ravi (2019a) compared the event rate of nearby FRB samples and those of cataclysmic progenitor events. The event rate of nearby FRBs exceeds the cataclysmic progenitor events, indicating that the FRB sample cannot be explained by only cataclysmic events. Hence, Ravi (2019a) concluded that most observed cases of FRBs must originate from sources that emit several bursts over their lifetimes.

The CHIME/FRB Collaboration et al. (2021) reported 474 non-repeating FRBs and 62 repeating bursts from 18 repeaters, implying the probability that a burst originates at a repeater is equal to $62/(62+474) = 11.5\%$. As exposure time increases (Ai et al. 2021), we expect more repeating and bright bursts will be detected. For instance, Herrmann (2021) reported a high-fluence FRB (334 Jy ms) from the FRB 20201124A repeating source with observation times of 90 hours. As a result of the small number of detections, the properties of repeating FRBs are poorly constrained (e.g., Fonseca et al. (2020)). This uncertainty includes the event rate and its dependence on flux density, the possibility of non-Poisson distribution of events (Oppermann et al. 2018), and the host environment of the FRB. With its all-sky, continuous sensitivity to high-fluence events, BURSTT will explore a unique parameter space for repeaters. Since BURSTT will detect ~ 100 high-fluence FRBs from the nearby Universe, the non-detections of repeats will shed some light on the underlying population using statistical methods.

Finding repeaters requires either high sensitivity or long exposure time. In order to detect more repeaters, we take the advantage of BURSTT's long exposure time (given by the large FoV) as a compensation to the sensitivity issue. We expect that BURSTT will detect high-fluence bursts from repeaters, and other telescopes with high sensitivity can do follow-up observations to detect more fainter bursts from the sources. For instance, the bright repeaters can then be readily followed-up by larger apertures, including the Five-hundred-meter Aperture Spherical Telescope (FAST), Giant Meterwave Radio Telescope (GMRT), Very Large Array (VLA). Historically, repetition rates increase rapidly with sensitivity, and thus we expect repeaters detected by the BURSTT to have the highest rates in follow-up campaigns.

With the high cadence, BURSTT may detect bright pulses from pulsars and rotating radio transients (Good et al. 2021), and further study their connections to FRBs (Bij et al. 2021; Thulasiram & Lin 2021; Majid et al. 2021).

2.4. An FRB telescope dedicated to the nearby Universe

Our plan to reveal the origin of FRBs is to explore the nearby Universe, because this maximizes the chance of detecting possible multi-wavelength and multi-messenger counterparts of FRBs, including FRB progenitors. For example, follow-up was key to the association of a repeating FRB with the Galactic magnetar SGR 1935+2154 (CHIME/FRB Collaboration et al. 2020; Bochenek et al. 2020b; Kirsten et al. 2021). This progenitor was identified because it is located nearby. Simultaneous X-ray emissions from SGR 1935+2154 were also detected with X-ray telescopes (e.g., Tavani et al. (2021)). This observed association gives hope that FRBs in nearby galaxies may also have detectable X-ray counterparts. (Li et al. 2021). BURSTT will monitor a large fraction of nearby galaxies.

An important wavelength range to examine for counterparts is the optical. No optical-FRB coincidence has found (Tominaga et al. 2018; MAGIC Collaboration et al. 2018) to date, and improved constraints would be very valuable,

because the expected flux density of the optical counterpart strongly depends on the physical mechanism of the FRB, e.g., the magnetosphere model predicts optical counterparts, whereas the maser model predicts a negligible flux density in optical (e.g., Yang et al. (2019); Yalinewich & Pen (2022)).

BURSTT is the ideal compliment to the current generation of multi-messenger detectors such as the Laser Interferometer Gravitational-Wave Observatory (LIGO) (Abbott et al. 2009), IceCube (Aartsen et al. 2017), and the Rubin Observatory’s Legacy Survey of Space and Time (LSST) (LSST Science Collaboration et al. 2009) which, like BURSTT, monitor the nearby Universe with near full-sky coverage. It will be instructive to search for FRBs associated with gravitational waves detected with the LIGO-Virgo-KAGRA Gravitational Wave Detector Network in near future (The LIGO Scientific Collaboration et al. 2022). Some FRB models predict an association with Gravitational-Wave (Wei et al. 2018) or neutrino counterparts (Metzger et al. 2020). If FRBs originate from neutron star mergers, which are known to generate gravitational waves (Abbott et al. 2017) and potentially neutrinos (Fang & Metzger 2017; Kimura et al. 2018), the expected time window of radio emission is on the millisecond time scale comparable to that of FRBs (e.g., Yamasaki et al. (2018)). So far, no FRB has been found in association with gravitational wave sources (e.g., Abbott et al. (2016); The LIGO Scientific Collaboration et al. (2022)). If no significant GW-FRB associations can be detected in future despite the greatly improved detection rate of BURSTT, the neutron star merger scenario for the origin of FRBs can be strongly constrained. Scenarios involving cosmic ray acceleration (e.g., Li et al. (2014); Metzger et al. (2020)) can produce neutrinos that can be detected by Large Volume Neutrino detectors, such as IceCube, KM3NeT (Adrián-Martínez et al. 2016), and Baikal-GVD (Avrorin et al. 2022). Although no neutrinos from FRBs have been detected so far, the probability of finding neutrino associations significantly improves with the total number of FRB detections (Aartsen et al. 2018, 2020). Such observations would bring clarity to the role of FRBs within the non-thermal universe and constrain the still unknown acceleration mechanisms of the highest energy cosmic rays.

In addition, the diffuse Galactic foreground is known to be pervasive, bright and dynamic, thus making it challenging to be observed properly. Only a few surveys have a large enough coverage to observe the low-frequency radio sky below 1 GHz (e.g. Haslam et al. 1981, 1982; Guzmán et al. 2011), including MSSS (Heald et al. 2015), GLEAM (Wayth et al. 2015) and TGSS (Intema et al. 2017). It is therefore complementary to generate low-frequency high resolution sky maps using e.g. the Long Wavelength Array (LWA) (e.g. Eastwood et al. 2018) and the Engineering Development Array 2 (EDA2) (e.g. Kriele et al. 2022). With the large FoV of BURSTT below 1 GHz, it has the potential to improve the removal of the Galactic foreground contamination in many Cosmic Microwave Background radiation and Epoch of Reionization works (see e.g. Ichiki (2014); Spinelli et al. (2021)).

3. BURSTT DESIGN

In this Section, we describe the initial designs of the BURSTT system with 256 antennas, which serves as a test-bed for BURSTT-2048. Our technology goal for BURSTT-256 is to optimize the system and compared component and algorithm designs.

3.1. Overview of the BURSTT Instrument and the telescope site

BURSTT-256 will consist of a combination one 256-antenna main station, and smaller outriggers at other sites in Taiwan and Hawaii.

We have surveyed several sites, and have permission to deploy the main station at the Fushan Botanical gardens ² in Northern Taiwan. Our survey indicates acceptable radio frequency interference (RFI) conditions at that site. We are continuing to survey other sites, sheltered from RFI, for the outrigger stations in Taiwan and surrounding islands as well as in Hawaii. The outriggers will each employ 64 antennas, allowing VLBI source localization (Leung et al. 2021; Mena-Parra et al. 2022; Cassanelli et al. 2022).

We will process an effective bandwidth of 400 MHz selected within the 300–800 MHz analog range through direct digital polyphase filterbanks (PFB). The CHIME/FRB team has demonstrated that processing a 400MHz bandwidth is practical (CHIME/FRB Collaboration et al. 2018). we would like to explore the FRB rate at frequencies below 400 MHz, the bottom of the CHIME band. Our design offers frequency agility. Should a shift in band improve the rate, BURSTT will be able to adapt through a simple software change.

² <https://fushan.tfri.gov.tw/en/index.php>

Table 1. The main properties of the BURSTT.

Quantity	Value	
Project	BURSTT-256	BURSTT-2048
SEFD	~ 5000 Jy	~ 600 Jy
Effective area	40-200 m ²	320-1600 m ²
Number of antennas (main station)	256	2048
(outrigger stations)		64
Polarization	single	
E-W FoV	$\sim 100^\circ$	
N-S FoV	$\sim 100^\circ$	
Daily exposure time	24 hrs (North pole)	
	~ 10 hrs (45°)	
	~ 7 hrs (Equator)	
Frequency range	300-800 MHz	TBD
Bandwidth	400 MHz	≥ 400 MHz
Number of frequency channels	1024	TBD
E-W baseline	~ 8000 km (Northern Taiwan to Hawaii)	
N-S baseline	~ 300 km (Northern to Southern Taiwan)	

Due to the modular nature, BURSTT is flexible to be expanded by deploying more antennas or outrigger stations. We plan to expand the main station from 256 antennas (BURSTT-256) to 2048 antennas (BURSTT-2048), and more outrigger stations could be deployed with a longer baselines, increasing the localization precision. The main properties of the BURSTT are summarized in Table 1.

For the BURSTT-256 project, the main station will search for bursts with fluence higher than 100 Jy ms, which is mentioned in Section 2.1. Assuming the duration of 1 ms and the bandwidth of 400 MHz, the corresponding S/N at the main station is 12. Once the main station detects a candidate burst, the data in the ring buffer in the outrigger will be copied out for the offline analysis. We expect a burst with a fluence of 100 Jy ms would yield an S/N at least of 6 in the cross-correlation analysis for the localization purpose.

We plan to use single-polarization antennas in BURSTT. These are simpler to design and build than dual-polarization antennas and optimization of the antenna-LNA match is more effective when only one polarization is involved. We plan to start with all antennas in one polarization direction within the main station array as this enhances sensitivity for linearly polarized source like FRBs. Later, we have the option to rotate some antennas to the orthogonal polarization if we determine that dual-polarization data is essential to test FRB source models.

Even in the initial configuration we plan to provide some polarized properties of all detected FRBs, such as rotation measure and polarization position angle swings (Masui et al. 2015) using two sub-stations with orthogonal polarization at one of the outrigger sites.

The back-end includes correlator hardware that will process the radio signals and accompanying software including fast Fourier transform (FFT) techniques and establish the capability to locate FRB events. Much of the development effort of the BURSTT program lies here, in the development and testing of real-time software. BURSTT will develop an upgraded version of the real-time processing digitizer and FRB search engines employed for CHIME (CHIME Collaboration et al. 2022).

An overview of the front- and back-ends of the main station is given in Figure 2. The front-end receives the signal from the sky through the bandpass (BP) filter and the noise amplifiers. The back-end digitizes the signals, performs the frequency-domain channelization, forms beams on the sky, and searches for FRBs. The hardware at outrigger stations will be similar to the main station, except that no beam-forming or FRB search will be performed. Rather the outriggers just record the arriving signal streams. This is discussed further in Sections 3.2 and 3.3.

3.2. FRONT-END DESIGN AND DEVELOPMENT

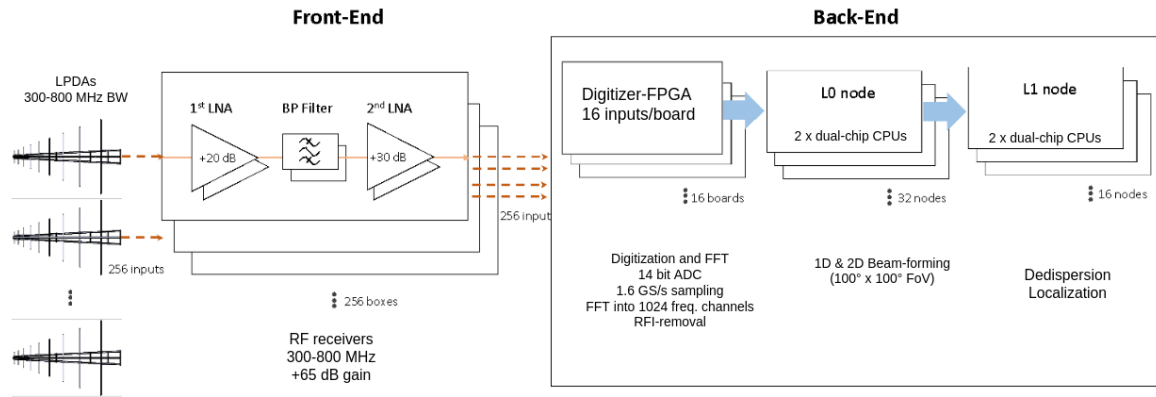


Figure 2. The system diagram of the BURSTT main station.

BURSTT will use Log-Periodic Dipole Array (LPDA) antennas. The LPDA antennas, which provide the required gain (7–9 dBi) with a simple structure, have been characterized and measured for use in numerous scientific and industrial applications. Millions of LPDAs have been deployed over the decades for use as home television antennas. Because LPDA antennas have a structure that can withstand strong winds, they are suitable for the environment in Taiwan, which experiences typhoons. Figure 3 shows the photo of various prototype antennas currently in development. The first one shown on the left is a standard design, which has been characterized well, but it is expensive to manufacture, and the long elements for low frequencies would be weak against strong winds. The second shown in the middle is the planar LPDA, which is a cost-effective design that simplifies the manufacturing process. However, since the elements have a long band-like structure, they can easily vibrate in the wind. The third design shown on the right is the planar LPDA attached to a quadrangular pyramid structure composed of insulator plates, which is cost-effective and raises the structure resonance frequency of the elements so that they can withstand strong winds. However, the structure can be heated by the sun, which can degrade the amplifier noise temperature. We will continue development and will test several prototypes in the field.

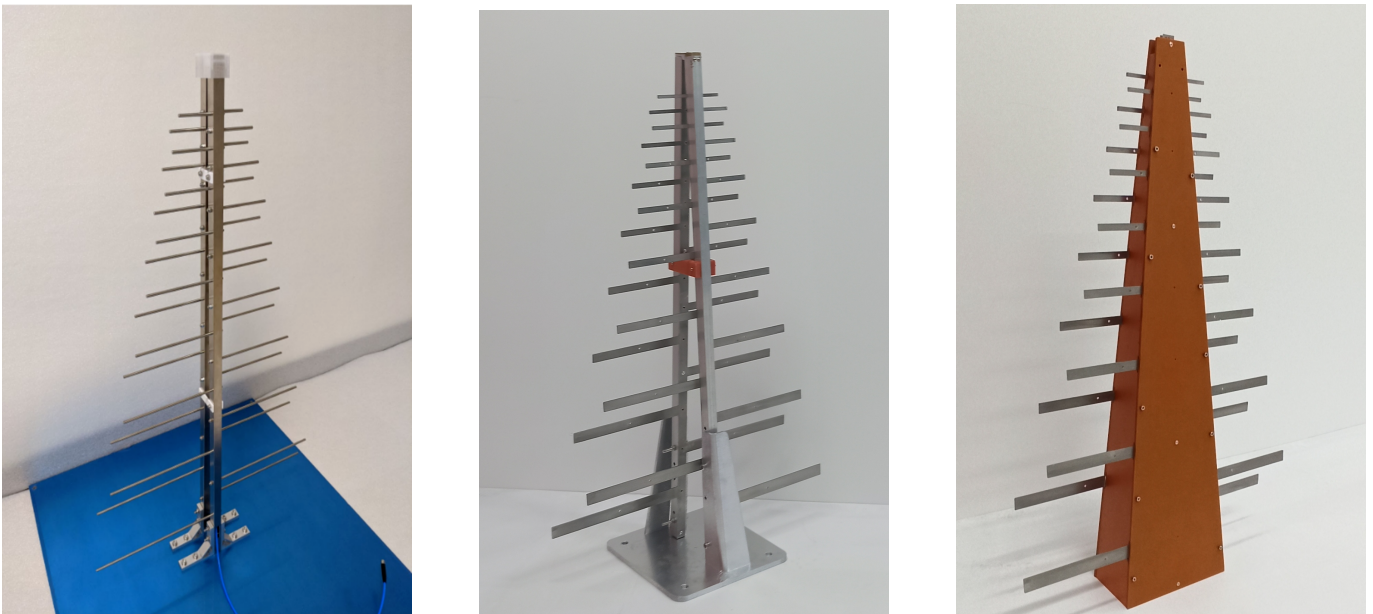


Figure 3. The photo of the prototype LPDA antennas in development. Standard LPDA (left), planar LPDA (middle), and planar LPDA on a quadrangular pyramid structure (right).

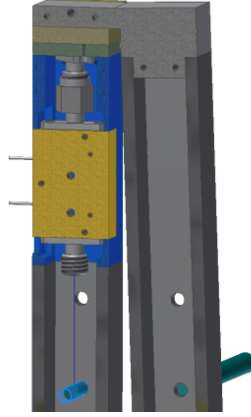


Figure 4. First-stage LNA (yellow) to be integrated into the LPDA: The feed point of the LPDA is directly connected to the input port of the first-stage LNA, the amplified signal is then transmitted to the second-stage FEE module by coaxial cable inside the support rod of the LPDA.

Received signals pass through the front-end electronics (FEE) before arriving at the digitizer. We will use a sampling rate of 1600 MHz, so our passband lies in the first Nyquist zone. This means no mixers or local oscillators are needed in the RF system. In order to minimize noise temperature due to transmission line losses, the first-stage low-noise amplifier (LNA) is closely integrated into the feed point of the LPDA as shown in Figure 4. The external second-stage FEE module consists of two equalizers cascaded with a second-stage amplifiers (LNAs) and filter modules to eliminate RFI at low frequencies and to prevent aliased detection of signals and noise above 800 MHz. Figure 5 shows the measured forward gain and the noise temperature (20-30 K) of a first-stage LNA we are developing. Comparing this to typical sky brightness temperature values, which fall with frequency from ~ 50 K at 300 MHz to ~ 6 K at 800 MHz, we see that the further effort to reduce LNA noise temperature can improve sensitivity, particularly at the high end of our frequency range. The required system gain is 65 dB, which is obtained by combining the first-stage LNA gain (25-30 dB) the second-stage amplifier assembly (35-40 dB) and slope-equalizer losses (-5 dB). We will continue to optimize the LNA design and plan to install an in-house developed low-noise amplifier in the 2048-antenna array.

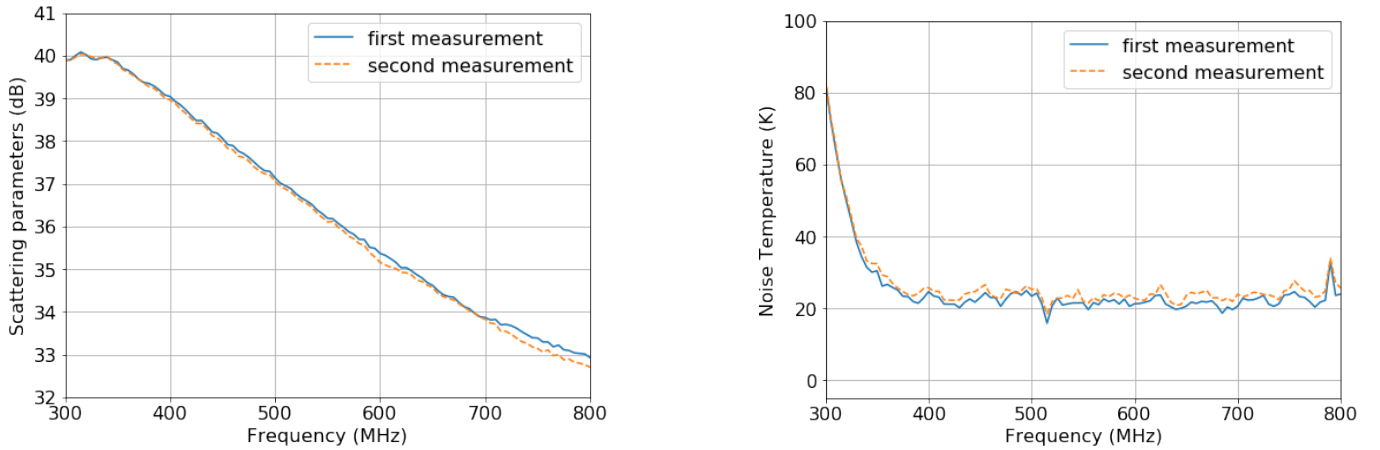


Figure 5. Measured performance of the two samples of the first-stage LNA, (left) measured forward gain with the output port connected with an equalizer, additional equalizer will be installed in the final system to provide ± 0.5 dB gain flatness over 350 – 800 MHz, (right) measured noise temperature.

The antenna array of BURSTT-256 station has a footprint of $32 \text{ m} \times 32 \text{ m}$, and the distance to the data acquisition (DAQ) hut where the digitizer is located is up to 50m, and which requires cable lengths ~ 60 m (Figure 6). When using the most popular and reliable coaxial cable, LMR-400, the transfer losses are -4 dB and -8 dB for 200 MHz and 900 MHz respectively, which can be corrected in the RF slope equalizer or in the correlator after channelization.

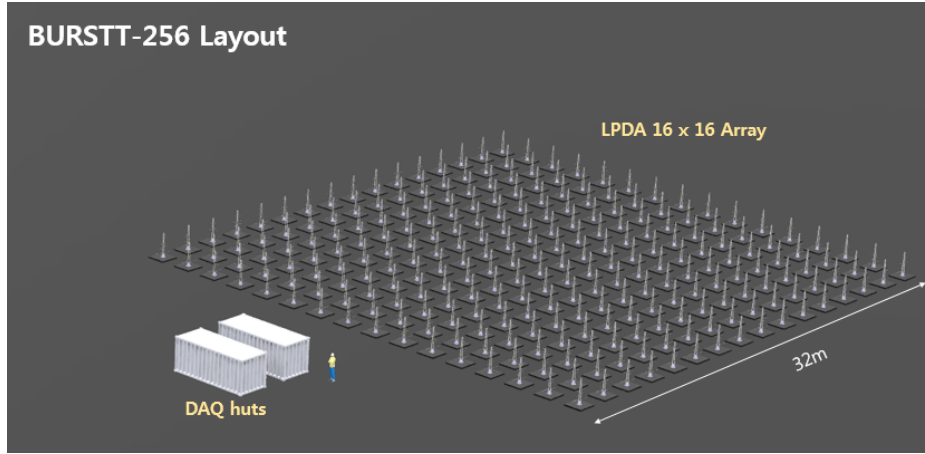


Figure 6. BURSTT 256-antenna array station layout.

Table 2. The FWHM of the beam pattern.

	300 MHz	400 MHz	600 MHz	800 MHz
E plane	58.0°	56.0°	58.0°	54.0°
H plane	80.0°	78.0°	77.0°	80.0°

3.2.1. The beam pattern

Figure 7 shows simulated far field radiation patterns of the LPDA antenna calculated using (i.e. the Ansys high-frequency structure simulator (HFSS) software). With the HFSS software, we utilize the finite element method to compute the EM field distribution of components. The 3 dB beam widths (FWHM) of the prototype LPDA antenna are around 80 degrees on the H plane and 60 degrees on the E plane from 300 MHz to 800 MHz (Table 2).

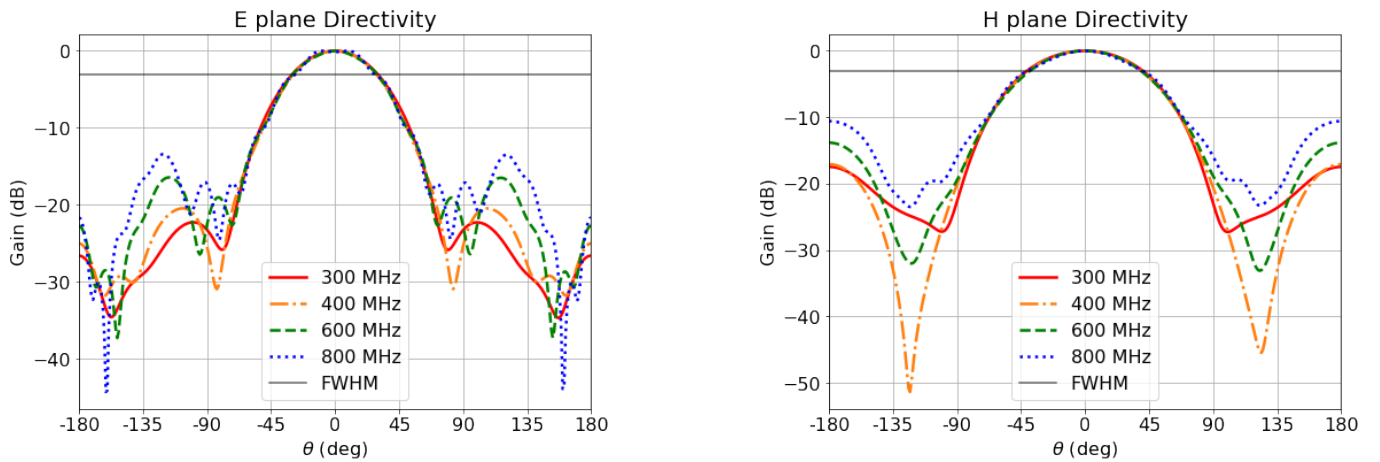


Figure 7. Normalized directivity of the prototype antenna simulated using HFSS, (left) the E plane directivity and (right) H plane directivity.

3.3. BACK-END DESIGN AND DEVELOPMENT

When the BURSTT main station detects a candidate FRB it sends a SAVE message to the outriggers, which then transfer recently-buffered data from RAM to disk. The outriggers and main station transmit the data to a VLBI

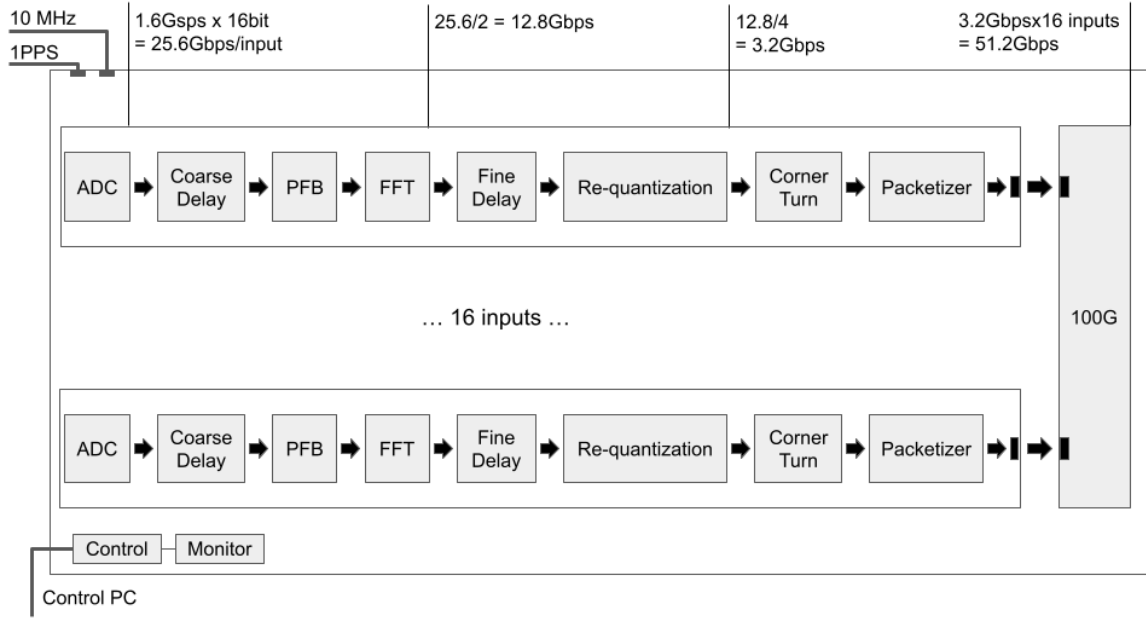


Figure 8. The functional block diagram of the BURSTT F-engine. Each FPGA-based RFSoc board will process 16 inputs with an initial bandwidth of 0–800 MHz. After channelization, a choice of 400 MHz bandwidth is retained. The re-quantization block further reduces the data rate by a factor of 4. Each board will send out a total of 51.2 Gbps of data over the 100G ethernet interface to a GPU processing node.

processing facility for localization processing. This process synthesizes an instrument with a nominal VLBI resolution $\lambda/(2D)$ of a 7,800 km \times 270 km baselines with 13 mas and 370 mas resolution in E-W and N-S respectively, allowing not only unique identification of each FRB’s host galaxy, but also ~ 100 parsec-scale localization of the FRB within that galaxy.

3.3.1. Digitizer and Engines

We are employing the Xilinx ZCU216 field programmable gate array (FPGA) boards as the platform of our digitizer and channelizer. The ZCU216 is equipped with a radio frequency system on chip (RFSoc) FPGA that can process 16 RF inputs. RFSoc systems include an embedded analog to digital converter (ADC) inside the FPGA chip, which simplifies wiring and saves physical space. This is the highest bandwidth RFSoc currently available. Figure 8 summarizes the functional block diagram of the RFSoc F-engine. We will be clocking the ADC at sampling rate 1600MHz for a Nyquist bandwidth of 800MHz. A poly-phase filter bank will channelize the data, forming 2048 bands of width ~ 390 kHz, and we will select 1024 of these for further analysis, choosing RFI-clear bands. We then re-quantized to resolution 4+4i bits to reduce the data rate. Gathering all the 16 input frequency domain data streams, a 100G Ethernet system will transmit the 100G UDP packets to the server for further data processing. The ADCs have 14-bit resolution substantially higher than the 8 bits sampling commonly used to date.

3.3.2. Preprocessing and RFI Mitigation

We discuss the steps of preprocessing in this section, including the RFI-removal techniques, beam-forming, and frequency channelization.

For BURSTT-256, the antennas will be organized into 16 columns, each with 16 antennas. The 16 antennas in a N-S column will be connected to one FPGA F-engine. It is thus efficient to perform 1D beamforming within the FPGA Ng et al. (2017). Each beam from the 16 F-engines is then similarly combined in the CPU-array to form the E-W direction beams, This process occurs independently for each frequency channel. This approach is similar in spirit to the 2D-FFT telescope (Tegmark & Zaldarriaga 2009) although with an implementation that is tailored to our F-engine design. For BURSTT-2048 a second layer of 2d spatial FFT will be carried out in the CPU array to synthesize all full-resolution beams.

The bandpass calibration and the system SEFD will be derived from observations of the Sun during the day. A pulsed broadband noise source will be used to monitor the gain variation during the night. Phase calibration will be achieved by using the many radio sources continuously available within the large FoV.

RFI Surveys in the Fushan candidate site shows that about 60% of the 300–800 MHz frequency range is free of noticeable RFI, while an additional 15% is affected by weak RFI. The FPGA F-engine offers a possibility of mitigating the weak RFI contamination using the using a spatial filtering technique applied to time streams from the antennas. (Kocz et al. 2010). The basic idea is that for a spatially fixed RFI source, the cross-correlation between any two antennas will record a distinct phase relation. The covariance matrix of all the antennas contains all the phase information one can measure with the array. Any source, not just the RFI sources, will contribute to the covariance matrix. However, for signals that are above the thermal noise, one can identify them by solving the eigenvalues and eigenvectors of the covariance matrix. This procedure is performed on each spectral channel independently. The antennas voltage data can be projected onto the eigenvectors to form the eigenmodes. The eigenmodes with the strongest variances (i.e. the largest eigenvalues) are assumed to be from the RFI source. It is therefore possible to remove the RFI contribution by nulling or zeroing out the RFI eigenmodes and deprojecting them back to the antenna data space. The antenna data after the RFI removal are passed onto the beamforming stage.

Figure 9 is an example of this technique applied to the TV station signal that was recorded in Fushan Botanical Garden (the main station site) with a 4-antenna test system. Three TV stations, each with a 6 MHz bandwidth, are within the recorded 40 MHz bandwidth. We note here that the eigenmode decomposition works better when the variance of the antennas are comparable. For this example, the four antennas have been normalized to the mean of the four antennas at each spectral channel. It is shown that for the TV signal centered on 581MHz, the signal is reduced by about 20 dB after nulling out the strongest eigenmode. The TV signal centered on 569 MHz is only reduced by a similar amount after nulling two of the strongest eigenmodes. It is possible that at Fushan, we are receiving the TV signals from multiple towers or that multi-path propagation is an important factor. As the project expands the testing to more sites and with more antennas, the RFI removal technique will be refined.

The performance of the RFI mitigation improves as the number of antennas is increased. Using the entire array in principle gives the best RFI nulling, but at substantial increase in the cost of the computation. To keep this system simple, we plan to update the RFI nulling solutions just once several hours or once a day. For the 16 antennas connected to one F-engine, applying the nulling solution is accomplished simply by multiplying the 16 antenna time streams for each frequency channel by a 16×16 complex matrix, similar to the beamforming operation. In fact, the two operations can be combined. Therefore, the RFI mitigation can be applied for each column of antennas at no additional real-time computational cost. Additional test will determine if 16-antenna RFI mitigation is sufficient or if more antennas should be combined to achieve the desired improvement.

3.3.3. *Dedispersion, search, and follow-up*

Searching for FRBs with unknown dispersion measure (DM) presents a challenge. This search has high computational cost and for BURSTT the search must be carried out real-time (Petroff et al. 2019), since the raw data rate is too high for disk storage. Search algorithms such as the Fast Dispersion Measure Transform (FDMT) (Zackay & Ofek 2017) or the tree-dedispersion algorithm (Taylor 1974; Masui et al. 2015; CHIME/FRB Collaboration et al. 2018) convert the intensity versus frequency and time into intensity versus DM and time data, along with the S/N estimates. Peaks in this data with S/N higher than 10 are initial FRB candidates. These dedispersion algorithms are well tested: the tree-dedispersion algorithm in real-time has been used by CHIME/FRB (CHIME/FRB Collaboration et al. 2018), the upgraded Molonglo Observatory Synthesis Telescope (UTMOST) (Farah et al. 2019), the Commensal Radio Astronomy FAST Survey (CRAFTS) (Niu et al. 2021), and Deep Synoptic Array 10 (DSA-10) (Ravi et al. 2019), and the FDMT algorithm in real-time has been implemented in ASKAP (Bannister et al. 2017).

Since the DM for the majority of FRBs is less than $1,000 \text{ pc cm}^{-3}$ (CHIME/Pulsar Collaboration et al. 2021) and the BURSTT will be searching for nearby FRBs, we will initially set the BURSTT DM range to 0 to $1,000 \text{ pc cm}^{-3}$.

In addition to transmitting automated SAVE messages to out outriggers, BURSTT will also send out real-time alert of the FRB events with an initial localization shortly after the detection to the community (Petroff et al. 2017; CHIME/FRB Collaboration et al. 2018), to allow rapid or retrospective multi-frequency and multi-messenger follow-up observations.

4. DISCUSSION AND SUMMARY

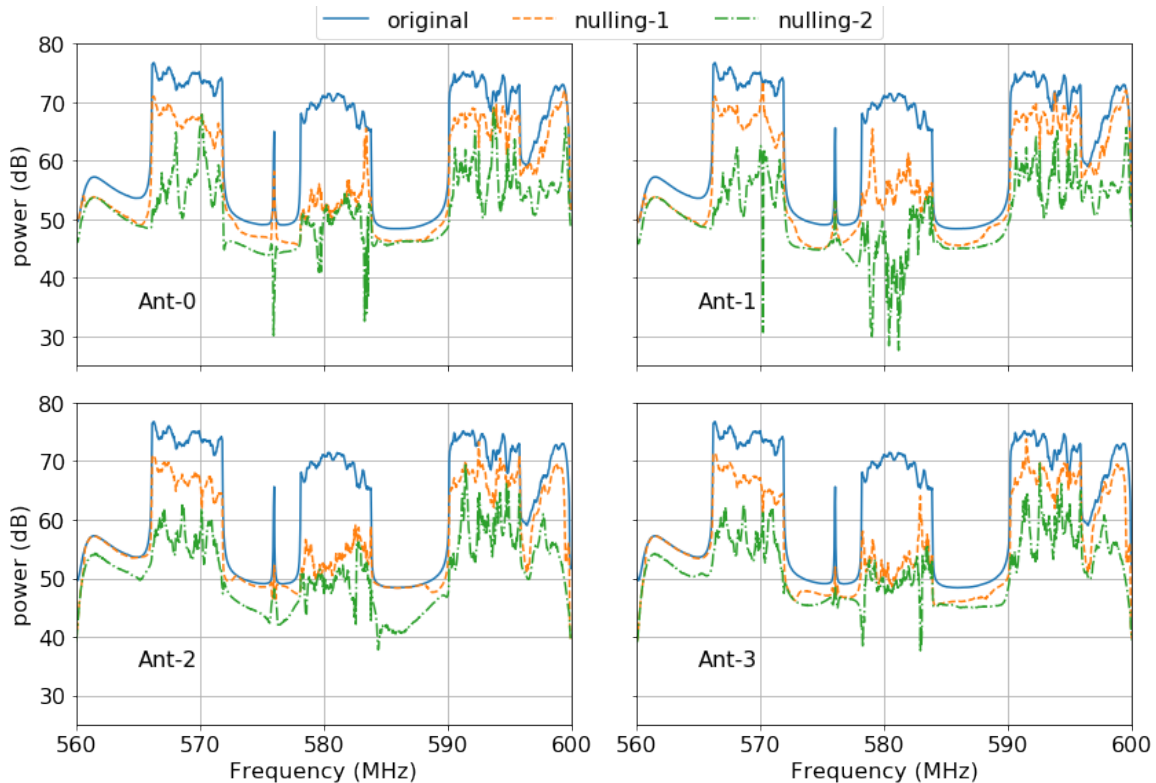


Figure 9. The RFI removal testing at the Fushan site. The four panels correspond to the four antennas. The blue solid line shows the originally received power as a function of observing frequency. The orange dotted line shows the received power after nulling of the strongest eigenmode. The green dashed line corresponds to the received power after nulling of strongest two eigenmodes.

Over 600 FRBs have been published since the first report in 2007 (Lorimer et al. 2007; Petroff et al. 2019; CHIME/FRB Collaboration et al. 2021), while the complex phenomena cannot be totally explained by theories (Pen 2018; Platts et al. 2019). The presence (or lack) of counterparts in other bands will provide critical constraints on both the emission mechanism and progenitor systems of FRBs (Popov & Pshirkov 2016; Cunningham et al. 2019). Candidate models such as compact object mergers and young magnetar flares yield very different predictions for multi-wavelength counterparts (Totani 2013; Popov & Postnov 2013; Pen 2018) yet progress has been slow due to a lack of precise and rapid FRB localizations to date.

BURSTT with a large FoV of $\sim 10^4$ deg² will monitor the whole visible sky for detecting and localizing ~ 100 bright and nearby FRBs per year. First, the large FoV yields a high cadence monitoring of FRBs, which is crucial to statistically understanding the repeater and the apparent one-off events. Second, the detection and localization of nearby FRBs offers the best chance for counterpart identification, which allows for timely follow-up observations at other wavelengths, including X-ray, infrared, etc. A large sample of ~ 100 bright FRBs per year will bring unprecedented new evidence about the nature of FRBs.

Understanding the physical processes through nearby and bright FRBs opens the possibility of further cosmological applications. Determining FRB host galaxies, and hence distances, moreover has the potential to enable large scale structure studies and unique determinations of the content of the intergalactic medium (IGM). This includes constraints on the location of the “missing baryons” in the Universe, whether in the IGM property, or in the halos of galaxies — the circumgalactic medium (e.g., McQuinn (2014); Ravi (2019b); Muñoz & Loeb (2018)). Some studies suggest that the structures of galaxy halos can be uniquely constrained by FRBs (Prochaska & Zheng 2019; Ocker et al. 2021), for comparison with models of galaxy evolution. Faraday rotation of polarized FRBs could constrain the origin and evolution of cosmic magnetism (Akhori et al. 2016). Uncertainties in FRBs’ dispersion measures have been proposed to constrain Einstein’s weak equivalence principle (Hashimoto et al. 2021).

The BURSTT design is scalable. Initially, 256 antennas will be deployed, which will help us to understand and improve the system. Because of its modular design, the telescope can be expanded simply by adding more main-station antennas, outriggers and correlation processors, with a corresponding increase in collecting area, localization precision, and sensitivity. In the BURSTT design we have eliminated the dishes, cylindrical reflectors, or RF-summed phased-arrays, used in other radio-telescopes. The BURSTT design therefore concentrates cost in the real-time signal-processing hardware. Most of this hardware is Commercial-Off-The-Shelf equipment, and is used for a wide range of general computing applications. Computing costs have fallen with Moore’s law for decades and continue to fall. BURSTT is therefore a technology pathfinder in an area that can be expected to grow both for scientific and financial reason. If computing costs continue to fall there is no reason to stop the expansion of BURSTT at 2048 elements, since further increases in collecting area allow an increase the volume and the redshift range of the survey.

Finally, in addition to deciphering the nature of the mysterious FRBs, BURSTT will open up a vast new discovery space for non-FRB surveys due to its unique all-sky collecting area. BURSTT can contribute to the study of self-triggering and reconstruction of cosmic-ray induced extensive air showers (Schröder 2017), as well as other extreme energy phenomena, such as Ultra-High Energy Cosmic Rays (Ackermann et al. 2022), and Ultra-High Energy neutrinos (Coleman et al. 2022). Moreover, BURSTT could also potentially contribute to LIGO counterparts (The LIGO Scientific Collaboration et al. 2022), Extreme Scattering Events (ESEs) (Kerr et al. 2018), 21cm absorbers (Margalit & Loeb 2016), pulsar searches (CHIME/Pulsar Collaboration et al. 2021), interplanetary scintillation (Hewish et al. 1964), etc. BURSTT will be a promising frontier of radio astronomy in the foreseeable future.

5. ACKNOWLEDGMENTS

The BURSTT project is supported by the National Science and Technology Council (NSTC) of Taiwan through Science Vanguard Research Program 111-2123-M-001-008-. U.L.P. receives support from Ontario Research Fund—research Excellence Program (ORF-RE), Natural Sciences and Engineering Research Council of Canada (NSERC) [funding reference number RGPIN-2019-067, CRD 523638-18, 555585-20], Canadian Institute for Advanced Research (CIFAR), Canadian Foundation for Innovation (CFI), the National Science Foundation of China (Grants No. 11929301), Thoth Technology Inc, Alexander von Humboldt Foundation, and the National Science and Technology Council (NSTC) of Taiwan (111-2123-M-001 -008 -, and 111-2811-M-001 -040 -). Computations were performed on the SOSCIP Consortium’s [Blue Gene/Q, Cloud Data Analytics, Agile and/or Large Memory System] computing platform(s). SOSCIP is funded by the Federal Economic Development Agency of Southern Ontario, the Province of Ontario, IBM Canada Ltd., Ontario Centres of Excellence, Mitacs and 15 Ontario academic member institutions. P.C. acknowledges the support by the National Science and Technology Council (NSTC) of Taiwan through the grant 111-2112-M-002-029- and by Leung Center for Cosmology and Particle Astrophysics (LeCosPA), National Taiwan University. TG acknowledges the supports by the National Science and Technology Council of Taiwan through grants 108-2628-M-007-004-MY3 and 111-2112-M-007 -021. T.H. acknowledges the support of the National Science and Technology Council of Taiwan through grants 110-2112-M-005-013-MY3 and 110-2112-M-007-034-. Y.C. acknowledges the support of the National Science and Technology Council of Taiwan through grant NSTC 111-2112-M-001-090-MY3. CPH acknowledges support from the National Science and Technology Council of Taiwan through grant MOST 109-2112-M-018-009-MY3. A.Y.L.O. is supported by the National Science and Technology Council (NSTC) of Taiwan (ROC) through the grants 111-2811-M-007-009 (PI: Prof. Ray-Kuang Lee, NTHU) and 110-2112-M-005-013-MY3 (PI: Prof. Tetsuya Hashimoto, NCHU).

REFERENCES

- Aartsen, M. G., Ackermann, M., Adams, J., et al. 2017, *Journal of Instrumentation*, 12, P03012, doi: [10.1088/1748-0221/12/03/P03012](https://doi.org/10.1088/1748-0221/12/03/P03012)
- . 2018, *ApJ*, 857, 117, doi: [10.3847/1538-4357/aab4f8](https://doi.org/10.3847/1538-4357/aab4f8)
- . 2020, *ApJ*, 890, 111, doi: [10.3847/1538-4357/ab564b](https://doi.org/10.3847/1538-4357/ab564b)
- Abbott, B. P., Abbott, R., Adhikari, R., et al. 2009, *Reports on Progress in Physics*, 72, 076901, doi: [10.1088/0034-4885/72/7/076901](https://doi.org/10.1088/0034-4885/72/7/076901)
- Abbott, B. P., Abbott, R., Abbott, T. D., et al. 2016, *PhRvD*, 93, 122003, doi: [10.1103/PhysRevD.93.122003](https://doi.org/10.1103/PhysRevD.93.122003)
- . 2017, *ApJL*, 848, L12, doi: [10.3847/2041-8213/aa91c9](https://doi.org/10.3847/2041-8213/aa91c9)
- Ackermann, M., Agarwalla, S. K., Alvarez-Muñiz, J., et al. 2022, arXiv e-prints, arXiv:2203.08096, <https://arxiv.org/abs/2203.08096>
- Adrián-Martínez, S., Ageron, M., Aharonian, F., et al. 2016, *Journal of Physics G Nuclear Physics*, 43, 084001, doi: [10.1088/0954-3899/43/8/084001](https://doi.org/10.1088/0954-3899/43/8/084001)

- Ai, S., Gao, H., & Zhang, B. 2021, *ApJL*, 906, L5, doi: [10.3847/2041-8213/abce9](https://doi.org/10.3847/2041-8213/abce9)
- Akahori, T., Ryu, D., & Gaensler, B. M. 2016, *ApJ*, 824, 105, doi: [10.3847/0004-637X/824/2/105](https://doi.org/10.3847/0004-637X/824/2/105)
- Anna-Thomas, R., Connor, L., Burke-Spolaor, S., et al. 2022, arXiv e-prints, arXiv:2202.11112. <https://arxiv.org/abs/2202.11112>
- Avrorin, A. V., Avrorin, A. D., Ayinutdinov, V. M., et al. 2022, *Soviet Journal of Experimental and Theoretical Physics*, 134, 399, doi: [10.1134/S10663776122040148](https://doi.org/10.1134/S10663776122040148)
- Bannister, K. W., Shannon, R. M., Macquart, J. P., et al. 2017, *ApJL*, 841, L12, doi: [10.3847/2041-8213/aa71ff](https://doi.org/10.3847/2041-8213/aa71ff)
- Bassa, C. G., Tendulkar, S. P., Adams, E. A. K., et al. 2017, *ApJL*, 843, L8, doi: [10.3847/2041-8213/aa7a0c](https://doi.org/10.3847/2041-8213/aa7a0c)
- Bhandari, S., Keane, E. F., Barr, E. D., et al. 2018, *MNRAS*, 475, 1427, doi: [10.1093/mnras/stx3074](https://doi.org/10.1093/mnras/stx3074)
- Bhandari, S., Sadler, E. M., Prochaska, J. X., et al. 2020, *ApJL*, 895, L37, doi: [10.3847/2041-8213/ab672e](https://doi.org/10.3847/2041-8213/ab672e)
- Bhandari, S., Heintz, K. E., Aggarwal, K., et al. 2022, *AJ*, 163, 69, doi: [10.3847/1538-3881/ac3aec](https://doi.org/10.3847/1538-3881/ac3aec)
- Bij, A., Lin, H.-H., Li, D., et al. 2021, *ApJ*, 920, 38, doi: [10.3847/1538-4357/ac1589](https://doi.org/10.3847/1538-4357/ac1589)
- Bilicki, M., Jarrett, T. H., Peacock, J. A., Cluver, M. E., & Steward, L. 2014, *ApJS*, 210, 9, doi: [10.1088/0067-0049/210/1/9](https://doi.org/10.1088/0067-0049/210/1/9)
- Bilicki, M., Peacock, J. A., Jarrett, T. H., et al. 2016, *ApJS*, 225, 5, doi: [10.3847/0067-0049/225/1/5](https://doi.org/10.3847/0067-0049/225/1/5)
- Bochenek, C. D., McKenna, D. L., Belov, K. V., et al. 2020a, *PASP*, 132, 034202, doi: [10.1088/1538-3873/ab63b3](https://doi.org/10.1088/1538-3873/ab63b3)
- Bochenek, C. D., Ravi, V., Belov, K. V., et al. 2020b, *Nature*, 587, 59, doi: [10.1038/s41586-020-2872-x](https://doi.org/10.1038/s41586-020-2872-x)
- Braun, R., Bonaldi, A., Bourke, T., Keane, E., & Wagg, J. 2019, arXiv e-prints, arXiv:1912.12699. <https://arxiv.org/abs/1912.12699>
- Cassanelli, T., Leung, C., Rahman, M., et al. 2022, *AJ*, 163, 65, doi: [10.3847/1538-3881/ac3d2f](https://doi.org/10.3847/1538-3881/ac3d2f)
- Chatterjee, S., Law, C. J., Wharton, R. S., et al. 2017, *Nature*, 541, 58, doi: [10.1038/nature20797](https://doi.org/10.1038/nature20797)
- Chen, B. H., Hashimoto, T., Goto, T., et al. 2022, *MNRAS*, 509, 1227, doi: [10.1093/mnras/stab2994](https://doi.org/10.1093/mnras/stab2994)
- CHIME Collaboration, Amiri, M., Bandura, K., et al. 2022, *ApJS*, 261, 29, doi: [10.3847/1538-4365/ac6fd9](https://doi.org/10.3847/1538-4365/ac6fd9)
- CHIME/FRB Collaboration, Amiri, M., Bandura, K., et al. 2018, *ApJ*, 863, 48, doi: [10.3847/1538-4357/aad188](https://doi.org/10.3847/1538-4357/aad188)
- Chime/Frb Collaboration, Amiri, M., Andersen, B. C., et al. 2020, *Nature*, 582, 351, doi: [10.1038/s41586-020-2398-2](https://doi.org/10.1038/s41586-020-2398-2)
- CHIME/FRB Collaboration, Andersen, B. C., Bandura, K. M., et al. 2020, *Nature*, 587, 54, doi: [10.1038/s41586-020-2863-y](https://doi.org/10.1038/s41586-020-2863-y)
- CHIME/FRB Collaboration, Amiri, M., Andersen, B. C., et al. 2021, *ApJS*, 257, 59, doi: [10.3847/1538-4365/ac33ab](https://doi.org/10.3847/1538-4365/ac33ab)
- CHIME/FRB Collaboration, Andersen, B. C., Bandura, K., Bhardwaj, M., et al. 2022, *Nature*, 607, 256, doi: [10.1038/s41586-022-04841-8](https://doi.org/10.1038/s41586-022-04841-8)
- CHIME/Pulsar Collaboration, Amiri, M., Bandura, K. M., et al. 2021, *ApJS*, 255, 5, doi: [10.3847/1538-4365/abfdcb](https://doi.org/10.3847/1538-4365/abfdcb)
- Coleman, A., Eser, J., Mayotte, E., et al. 2022, arXiv e-prints, arXiv:2205.05845. <https://arxiv.org/abs/2205.05845>
- Connor, L., Lin, H.-H., Masui, K., et al. 2016, *MNRAS*, 460, 1054, doi: [10.1093/mnras/stw907](https://doi.org/10.1093/mnras/stw907)
- Connor, L., Shila, K. A., Kulkarni, S. R., et al. 2021, *PASP*, 133, 075001, doi: [10.1088/1538-3873/ac0bcc](https://doi.org/10.1088/1538-3873/ac0bcc)
- Cunningham, V., Cenko, S. B., Burns, E., et al. 2019, *ApJ*, 879, 40, doi: [10.3847/1538-4357/ab2235](https://doi.org/10.3847/1538-4357/ab2235)
- Cutri, R. M., Skrutskie, M. F., van Dyk, S., et al. 2003, 2MASS All Sky Catalog of point sources.
- Dai, S., Feng, Y., Yang, Y. P., et al. 2022, arXiv e-prints, arXiv:2203.08151. <https://arxiv.org/abs/2203.08151>
- Dey, A., Schlegel, D. J., Lang, D., et al. 2019, *AJ*, 157, 168, doi: [10.3847/1538-3881/ab089d](https://doi.org/10.3847/1538-3881/ab089d)
- Eastwood, M. W., Anderson, M. M., Monroe, R. M., et al. 2018, *AJ*, 156, 32, doi: [10.3847/1538-3881/aac721](https://doi.org/10.3847/1538-3881/aac721)
- Fang, K., & Metzger, B. D. 2017, *ApJ*, 849, 153, doi: [10.3847/1538-4357/aa8b6a](https://doi.org/10.3847/1538-4357/aa8b6a)
- Farah, W., Flynn, C., Bailes, M., et al. 2019, *MNRAS*, 488, 2989, doi: [10.1093/mnras/stz1748](https://doi.org/10.1093/mnras/stz1748)
- Fonseca, E., Andersen, B. C., Bhardwaj, M., et al. 2020, *ApJL*, 891, L6, doi: [10.3847/2041-8213/ab7208](https://doi.org/10.3847/2041-8213/ab7208)
- Good, D. C., Andersen, B. C., Chawla, P., et al. 2021, *ApJ*, 922, 43, doi: [10.3847/1538-4357/ac1da6](https://doi.org/10.3847/1538-4357/ac1da6)
- Guzmán, A. E., May, J., Alvarez, H., & Maeda, K. 2011, *A&A*, 525, A138, doi: [10.1051/0004-6361/200913628](https://doi.org/10.1051/0004-6361/200913628)
- Hashimoto, T., Goto, T., Wang, T.-W., et al. 2019, *MNRAS*, 488, 1908, doi: [10.1093/mnras/stz1715](https://doi.org/10.1093/mnras/stz1715)
- Hashimoto, T., Goto, T., On, A. Y. L., et al. 2020, *MNRAS*, 498, 3927, doi: [10.1093/mnras/staa2490](https://doi.org/10.1093/mnras/staa2490)
- Hashimoto, T., Goto, T., Santos, D. J. D., et al. 2021, *PhRvD*, 104, 124026, doi: [10.1103/PhysRevD.104.124026](https://doi.org/10.1103/PhysRevD.104.124026)
- Haslam, C. G. T., Klein, U., Salter, C. J., et al. 1981, *A&A*, 100, 209
- Haslam, C. G. T., Salter, C. J., Stoffel, H., & Wilson, W. E. 1982, *A&AS*, 47, 1
- Heald, G. H., Pizzo, R. F., Orrú, E., et al. 2015, *A&A*, 582, A123, doi: [10.1051/0004-6361/201425210](https://doi.org/10.1051/0004-6361/201425210)

- Heintz, K. E., Prochaska, J. X., Simha, S., et al. 2020, *ApJ*, 903, 152, doi: [10.3847/1538-4357/abb6fb](https://doi.org/10.3847/1538-4357/abb6fb)
- Herrmann, W. 2021, *The Astronomer's Telegram*, 14556, 1
- Hewish, A., Scott, P. F., & Wills, D. 1964, *Nature*, 203, 1214, doi: [10.1038/2031214a0](https://doi.org/10.1038/2031214a0)
- Ichiki, K. 2014, *Progress of Theoretical and Experimental Physics*, 2014, 06B109, doi: [10.1093/ptep/ptu065](https://doi.org/10.1093/ptep/ptu065)
- Intema, H. T., Jagannathan, P., Mooley, K. P., & Frail, D. A. 2017, *A&A*, 598, A78, doi: [10.1051/0004-6361/201628536](https://doi.org/10.1051/0004-6361/201628536)
- Jiang, P., Yue, Y., Gan, H., et al. 2019, *Science China Physics, Mechanics, and Astronomy*, 62, 959502, doi: [10.1007/s11433-018-9376-1](https://doi.org/10.1007/s11433-018-9376-1)
- Josephy, A., Chawla, P., Curtin, A. P., et al. 2021, *ApJ*, 923, 2, doi: [10.3847/1538-4357/ac33ad](https://doi.org/10.3847/1538-4357/ac33ad)
- Karachentsev, I. D., Makarov, D. I., & Kaisina, E. I. 2013, *AJ*, 145, 101, doi: [10.1088/0004-6256/145/4/101](https://doi.org/10.1088/0004-6256/145/4/101)
- Kerr, M., Coles, W. A., Ward, C. A., et al. 2018, *MNRAS*, 474, 4637, doi: [10.1093/mnras/stx3101](https://doi.org/10.1093/mnras/stx3101)
- Kimura, S. S., Murase, K., Bartos, I., et al. 2018, *PhRvD*, 98, 043020, doi: [10.1103/PhysRevD.98.043020](https://doi.org/10.1103/PhysRevD.98.043020)
- Kirsten, F., Snelders, M. P., Jenkins, M., et al. 2021, *Nature Astronomy*, 5, 414, doi: [10.1038/s41550-020-01246-3](https://doi.org/10.1038/s41550-020-01246-3)
- Kirsten, F., Marcote, B., Nimmo, K., et al. 2022, *Nature*, 602, 585, doi: [10.1038/s41586-021-04354-w](https://doi.org/10.1038/s41586-021-04354-w)
- Kocz, J., Briggs, F. H., & Reynolds, J. 2010, *AJ*, 140, 2086, doi: [10.1088/0004-6256/140/6/2086](https://doi.org/10.1088/0004-6256/140/6/2086)
- Kriele, M. A., Wayth, R. B., Bentum, M. J., Juswardy, B., & Trott, C. M. 2022, *PASA*, 39, e017, doi: [10.1017/pasa.2022.2](https://doi.org/10.1017/pasa.2022.2)
- Law, C. J., Bower, G. C., Burke-Spolaor, S., et al. 2018, *ApJS*, 236, 8, doi: [10.3847/1538-4365/aab77b](https://doi.org/10.3847/1538-4365/aab77b)
- Leung, C., Mena-Parra, J., Masui, K., et al. 2021, *AJ*, 161, 81, doi: [10.3847/1538-3881/abd174](https://doi.org/10.3847/1538-3881/abd174)
- Leung, C., Kader, Z., Masui, K. W., et al. 2022, *PhRvD*, 106, 043017, doi: [10.1103/PhysRevD.106.043017](https://doi.org/10.1103/PhysRevD.106.043017)
- Li, C. K., Lin, L., Xiong, S. L., et al. 2021, *Nature Astronomy*, 5, 378, doi: [10.1038/s41550-021-01302-6](https://doi.org/10.1038/s41550-021-01302-6)
- Li, X., Zhou, B., He, H.-N., Fan, Y.-Z., & Wei, D.-M. 2014, *ApJ*, 797, 33, doi: [10.1088/0004-637X/797/1/33](https://doi.org/10.1088/0004-637X/797/1/33)
- Li, Y., & Zhang, B. 2020, *ApJL*, 899, L6, doi: [10.3847/2041-8213/aba907](https://doi.org/10.3847/2041-8213/aba907)
- Liu, B., Li, Z., Gao, H., & Zhu, Z.-H. 2019, *PhRvD*, 99, 123517, doi: [10.1103/PhysRevD.99.123517](https://doi.org/10.1103/PhysRevD.99.123517)
- Lorimer, D. R., Bailes, M., McLaughlin, M. A., Narkevic, D. J., & Crawford, F. 2007, *Science*, 318, 777, doi: [10.1126/science.1147532](https://doi.org/10.1126/science.1147532)
- LSST Science Collaboration, Abell, P. A., Allison, J., et al. 2009, *arXiv e-prints*, arXiv:0912.0201. <https://arxiv.org/abs/0912.0201>
- Luo, R., Lee, K., Lorimer, D. R., & Zhang, B. 2018, *MNRAS*, 481, 2320, doi: [10.1093/mnras/sty2364](https://doi.org/10.1093/mnras/sty2364)
- Macquart, J.-P., Bailes, M., Bhat, N. D. R., et al. 2010, *PASA*, 27, 272, doi: [10.1071/AS09082](https://doi.org/10.1071/AS09082)
- Macquart, J. P., Prochaska, J. X., McQuinn, M., et al. 2020, *Nature*, 581, 391, doi: [10.1038/s41586-020-2300-2](https://doi.org/10.1038/s41586-020-2300-2)
- MAGIC Collaboration, Acciari, V. A., Ansoldi, S., et al. 2018, *MNRAS*, 481, 2479, doi: [10.1093/mnras/sty2422](https://doi.org/10.1093/mnras/sty2422)
- Majid, W. A., Pearlman, A. B., Prince, T. A., et al. 2021, *ApJL*, 919, L6, doi: [10.3847/2041-8213/ac1921](https://doi.org/10.3847/2041-8213/ac1921)
- Marcote, B., Paragi, Z., Hessels, J. W. T., et al. 2017, *ApJL*, 834, L8, doi: [10.3847/2041-8213/834/2/L8](https://doi.org/10.3847/2041-8213/834/2/L8)
- Marcote, B., Nimmo, K., Hessels, J. W. T., et al. 2020, *Nature*, 577, 190, doi: [10.1038/s41586-019-1866-z](https://doi.org/10.1038/s41586-019-1866-z)
- Margalit, B., & Loeb, A. 2016, *MNRAS*, 460, L25, doi: [10.1093/mnras/1slw068](https://doi.org/10.1093/mnras/1slw068)
- Masui, K., Lin, H.-H., Sievers, J., et al. 2015, *Nature*, 528, 523, doi: [10.1038/nature15769](https://doi.org/10.1038/nature15769)
- McQuinn, M. 2014, *ApJL*, 780, L33, doi: [10.1088/2041-8205/780/2/L33](https://doi.org/10.1088/2041-8205/780/2/L33)
- Mena-Parra, J., Leung, C., Cary, S., et al. 2022, *AJ*, 163, 48, doi: [10.3847/1538-3881/ac397a](https://doi.org/10.3847/1538-3881/ac397a)
- Metzger, B. D., Fang, K., & Margalit, B. 2020, *ApJL*, 902, L22, doi: [10.3847/2041-8213/abbb88](https://doi.org/10.3847/2041-8213/abbb88)
- Michilli, D., Seymour, A., Hessels, J. W. T., et al. 2018, *Nature*, 553, 182, doi: [10.1038/nature25149](https://doi.org/10.1038/nature25149)
- Muñoz, J. B., Kovetz, E. D., Dai, L., & Kamionkowski, M. 2016, *PhRvL*, 117, 091301, doi: [10.1103/PhysRevLett.117.091301](https://doi.org/10.1103/PhysRevLett.117.091301)
- Muñoz, J. B., & Loeb, A. 2018, *PhRvD*, 98, 103518, doi: [10.1103/PhysRevD.98.103518](https://doi.org/10.1103/PhysRevD.98.103518)
- Newburgh, L. B., Bandura, K., Bucher, M. A., et al. 2016, in *Society of Photo-Optical Instrumentation Engineers (SPIE) Conference Series*, Vol. 9906, *Ground-based and Airborne Telescopes VI*, ed. H. J. Hall, R. Gilmozzi, & H. K. Marshall, 99065X, doi: [10.1117/12.2234286](https://doi.org/10.1117/12.2234286)
- Ng, C., Vanderlinde, K., Paradise, A., et al. 2017, in *XXXII International Union of Radio Science General Assembly & Scientific Symposium (URSI GASS) 2017*, 4, doi: [10.23919/URSIGASS.2017.8105318](https://doi.org/10.23919/URSIGASS.2017.8105318)
- Niu, C.-H., Li, D., Luo, R., et al. 2021, *ApJL*, 909, L8, doi: [10.3847/2041-8213/abe7f0](https://doi.org/10.3847/2041-8213/abe7f0)
- Niu, C. H., Aggarwal, K., Li, D., et al. 2022, *Nature*, 606, 873, doi: [10.1038/s41586-022-04755-5](https://doi.org/10.1038/s41586-022-04755-5)
- Ocker, S. K., Cordes, J. M., & Chatterjee, S. 2021, *ApJ*, 911, 102, doi: [10.3847/1538-4357/abeb6e](https://doi.org/10.3847/1538-4357/abeb6e)
- Oppermann, N., Yu, H.-R., & Pen, U.-L. 2018, *MNRAS*, 475, 5109, doi: [10.1093/mnras/sty004](https://doi.org/10.1093/mnras/sty004)
- Pen, U.-L. 2018, *Nature Astronomy*, 2, 842, doi: [10.1038/s41550-018-0620-z](https://doi.org/10.1038/s41550-018-0620-z)

- Petroff, E., Hessels, J. W. T., & Lorimer, D. R. 2019, *A&A Rv*, 27, 4, doi: [10.1007/s00159-019-0116-6](https://doi.org/10.1007/s00159-019-0116-6)
- Petroff, E., van Straten, W., Johnston, S., et al. 2014, *ApJL*, 789, L26, doi: [10.1088/2041-8205/789/2/L26](https://doi.org/10.1088/2041-8205/789/2/L26)
- Petroff, E., Barr, E. D., Jameson, A., et al. 2016, *PASA*, 33, e045, doi: [10.1017/pasa.2016.35](https://doi.org/10.1017/pasa.2016.35)
- Petroff, E., Houben, L., Bannister, K., et al. 2017, arXiv e-prints, arXiv:1710.08155. <https://arxiv.org/abs/1710.08155>
- Piro, L., Bruni, G., Troja, E., et al. 2021, *A&A*, 656, L15, doi: [10.1051/0004-6361/202141903](https://doi.org/10.1051/0004-6361/202141903)
- Platts, E., Weltman, A., Walters, A., et al. 2019, *PhR*, 821, 1, doi: [10.1016/j.physrep.2019.06.003](https://doi.org/10.1016/j.physrep.2019.06.003)
- Popov, S. B., & Postnov, K. A. 2013, arXiv e-prints, arXiv:1307.4924. <https://arxiv.org/abs/1307.4924>
- Popov, S. B., & Pshirkov, M. S. 2016, *MNRAS*, 462, L16, doi: [10.1093/mnrasl/slw118](https://doi.org/10.1093/mnrasl/slw118)
- Prochaska, J. X., & Zheng, Y. 2019, *MNRAS*, 485, 648, doi: [10.1093/mnras/stz261](https://doi.org/10.1093/mnras/stz261)
- Rafiei-Ravandi, M., Smith, K. M., Li, D., et al. 2021, *ApJ*, 922, 42, doi: [10.3847/1538-4357/ac1dab](https://doi.org/10.3847/1538-4357/ac1dab)
- Rajwade, K., Stappers, B., Williams, C., et al. 2021, arXiv e-prints, arXiv:2103.08410. <https://arxiv.org/abs/2103.08410>
- Rajwade, K. M., Mickaliger, M. B., Stappers, B. W., et al. 2020, *MNRAS*, 495, 3551, doi: [10.1093/mnras/staa1237](https://doi.org/10.1093/mnras/staa1237)
- Ravi, V. 2019a, *Nature Astronomy*, 3, 928, doi: [10.1038/s41550-019-0831-y](https://doi.org/10.1038/s41550-019-0831-y)
- . 2019b, *ApJ*, 872, 88, doi: [10.3847/1538-4357/aafb30](https://doi.org/10.3847/1538-4357/aafb30)
- Ravi, V., Catha, M., D'Addario, L., et al. 2019, *Nature*, 572, 352, doi: [10.1038/s41586-019-1389-7](https://doi.org/10.1038/s41586-019-1389-7)
- Schröder, F. G. 2017, *Progress in Particle and Nuclear Physics*, 93, 1, doi: [10.1016/j.pnpnp.2016.12.002](https://doi.org/10.1016/j.pnpnp.2016.12.002)
- Shin, K., Masui, K. W., Bhardwaj, M., et al. 2022, arXiv e-prints, arXiv:2207.14316. <https://arxiv.org/abs/2207.14316>
- Slosar, A., Ahmed, Z., Alonso, D., et al. 2019, in *Bulletin of the American Astronomical Society*, Vol. 51, 53. <https://arxiv.org/abs/1907.12559>
- Spinelli, M., Bernardi, G., Garsden, H., et al. 2021, *MNRAS*, 505, 1575, doi: [10.1093/mnras/stab1363](https://doi.org/10.1093/mnras/stab1363)
- Spitler, L. G., Scholz, P., Hessels, J. W. T., et al. 2016, *Nature*, 531, 202, doi: [10.1038/nature17168](https://doi.org/10.1038/nature17168)
- Tavani, M., Casentini, C., Ursi, A., et al. 2021, *Nature Astronomy*, 5, 401, doi: [10.1038/s41550-020-01276-x](https://doi.org/10.1038/s41550-020-01276-x)
- Taylor, J. H. 1974, *A&AS*, 15, 367
- Tegmark, M., & Zaldarriaga, M. 2009, *PhRvD*, 79, 083530, doi: [10.1103/PhysRevD.79.083530](https://doi.org/10.1103/PhysRevD.79.083530)
- Tendulkar, S. P., Bassa, C. G., Cordes, J. M., et al. 2017, *ApJL*, 834, L7, doi: [10.3847/2041-8213/834/2/L7](https://doi.org/10.3847/2041-8213/834/2/L7)
- The LIGO Scientific Collaboration, the Virgo Collaboration, the KAGRA Collaboration, et al. 2022, arXiv e-prints, arXiv:2203.12038. <https://arxiv.org/abs/2203.12038>
- Thulasiram, P., & Lin, H.-H. 2021, *MNRAS*, 508, 1947, doi: [10.1093/mnras/stab2692](https://doi.org/10.1093/mnras/stab2692)
- Tominaga, N., Niino, Y., Totani, T., et al. 2018, *PASJ*, 70, 103, doi: [10.1093/pasj/psy101](https://doi.org/10.1093/pasj/psy101)
- Torchinsky, S. A., Broderick, J. W., Gunst, A., Faulkner, A. J., & van Cappellen, W. 2016, arXiv e-prints, arXiv:1610.00683. <https://arxiv.org/abs/1610.00683>
- Totani, T. 2013, *PASJ*, 65, L12, doi: [10.1093/pasj/65.5.L12](https://doi.org/10.1093/pasj/65.5.L12)
- Vanderlinde, K., Liu, A., Gaensler, B., et al. 2019, in *Canadian Long Range Plan for Astronomy and Astrophysics White Papers*, Vol. 2020, 28, doi: [10.5281/zenodo.3765414](https://doi.org/10.5281/zenodo.3765414)
- Wayth, R. B., Lenc, E., Bell, M. E., et al. 2015, *PASA*, 32, e025, doi: [10.1017/pasa.2015.26](https://doi.org/10.1017/pasa.2015.26)
- Wei, J.-J., Gao, H., Wu, X.-F., & Mészáros, P. 2015, *PhRvL*, 115, 261101, doi: [10.1103/PhysRevLett.115.261101](https://doi.org/10.1103/PhysRevLett.115.261101)
- Wei, J.-J., Wu, X.-F., & Gao, H. 2018, *ApJL*, 860, L7, doi: [10.3847/2041-8213/aac8e2](https://doi.org/10.3847/2041-8213/aac8e2)
- Yalinewich, A., & Pen, U.-L. 2022, *MNRAS*, 515, 5682, doi: [10.1093/mnras/stac2087](https://doi.org/10.1093/mnras/stac2087)
- Yamasaki, S., Totani, T., & Kiuchi, K. 2018, *PASJ*, 70, 39, doi: [10.1093/pasj/psy029](https://doi.org/10.1093/pasj/psy029)
- Yang, Y.-P., Zhang, B., & Wei, J.-Y. 2019, *ApJ*, 878, 89, doi: [10.3847/1538-4357/ab1fe2](https://doi.org/10.3847/1538-4357/ab1fe2)
- Zackay, B., & Ofek, E. O. 2017, *ApJ*, 835, 11, doi: [10.3847/1538-4357/835/1/11](https://doi.org/10.3847/1538-4357/835/1/11)